

Efficient Discovery of Approximate Causal Abstractions via Neural Mechanism Sparsification

Amir Asiaee

AMIR.ASIAEETAHERI@VUMC.ORG

Department of Biostatistics, Vanderbilt University Medical Center, Nashville, TN, USA

Abstract

Neural networks are hypothesized to implement interpretable causal mechanisms, yet verifying this requires finding a *causal abstraction*—a simpler, high-level Structural Causal Model (SCM) faithful to the network under interventions. Discovering such abstractions is hard: it typically demands brute-force interchange interventions or retraining. We reframe the problem by viewing structured pruning as a search over approximate abstractions. Treating a trained network as a deterministic SCM, we derive an *Interventional Risk* objective whose second-order expansion yields closed-form criteria for replacing units with constants or folding them into neighbors. Under uniform curvature, our score reduces to activation variance, recovering variance-based pruning as a special case while clarifying when it fails. The resulting procedure efficiently extracts sparse, intervention-faithful abstractions from pretrained networks, which we validate via interchange interventions.

Keywords: Causal model reduction; structural causal models; causal abstraction; interventions; structured pruning; mechanistic interpretability

1. Introduction

Deep neural networks achieve impressive predictive accuracy but resist mechanistic interpretation. A core difficulty is that observational performance alone cannot distinguish models implementing stable, generalizable algorithms from those exploiting spurious training-set regularities. This has spurred interest in *mechanistic interpretability* and *causal abstraction*: extracting faithful high-level causal descriptions of how models compute their outputs (Olah et al., 2020; Geiger et al., 2021, 2025).

Causal abstraction formalizes when a complex, low-level causal model admits a simpler high-level description via a state map τ and an intervention map ω . The key requirement is *commutativity*: intervening at the high level and refining back should match intervening at the low level and then abstracting (Rubenstein et al., 2017; Beckers and Halpern, 2019; Beckers et al., 2020). For neural networks, *interchange interventions* operationalize this test, and *interchange intervention accuracy* (IIA) quantifies how well commutativity holds (Geiger et al., 2021, 2025). Notably, networks can score well on behavioral metrics while failing these interventional tests, revealing mechanistic brittleness invisible to standard evaluation (Geiger et al., 2022).

Most prior work assumes access to a candidate high-level model and focuses on *verifying* the abstraction (Geiger et al., 2021, 2024). For large pretrained networks, the harder problem is *discovery*: identifying which internal variables support a faithful high-level description. The search space is combinatorial, and directly optimizing IIA is expensive.

We propose a constructive approach. Viewing a trained feedforward network as a deterministic SCM over its activations (Pearl, 2009), we search over abstractions implemented by *mechanism replacement*: substituting selected units with constants (hard interventions) or affine functions of

retained units (soft interventions) (Massidda et al., 2023). These operations produce an explicit reduced SCM that can be compiled into a smaller dense network. To make discovery tractable, we approximate the induced change in task loss via a second-order Taylor expansion, yielding closed-form replacement parameters and per-unit importance scores. Candidate abstractions identified this way can then be verified with interchange interventions.

Contributions. We develop a framework for discovering causal abstractions of pretrained neural networks via mechanism replacement, connecting causal abstraction theory to structured pruning. Our main contributions are:

1. **Constructive abstraction discovery.** We formalize the problem of finding a reduced SCM (M_H, τ, ω) that approximately commutes with a trained network on a specified intervention family. Unlike prior work that assumes a candidate high-level model, we *discover* the abstraction by searching over mechanism replacements—hard interventions (constant assignment) and soft interventions (affine surrogates)—that remove or fold internal variables while preserving interventional behavior.
2. **Tractable second-order surrogate.** Direct optimization of interchange intervention accuracy is expensive. We derive a quadratic approximation to the task-loss change induced by mechanism replacement, yielding: (a) a closed-form optimal replacement constant c_j^* that combines a curvature-weighted mean with a gradient correction, and (b) a per-unit score s_j quantifying the minimal cost of replacing each unit. These can be computed in a single autodiff pass over a calibration set.
3. **Exact compilation.** We show that constant and affine mechanism replacements can be *compiled* into standard dense networks via bias folding and weight redistribution, without runtime masking or architectural changes. The compiled network is an exact functional transformation of the intervened SCM, making the discovered abstraction directly operational.
4. **Connection to variance-based pruning.** Under stationarity (zero mean gradient) and uniform curvature, our optimal constant reduces to the activation mean and our score reduces to activation variance. This recovers variance-based structured pruning (Berisha et al., 2025) as a special case, providing a causal-abstraction interpretation of an existing heuristic while explaining when it succeeds (uniform curvature) and when it fails (e.g., under reparameterization).
5. **Empirical validation.** We demonstrate that abstractions discovered via our Logit-MSE fidelity score achieve higher interchange intervention accuracy than variance-based methods, particularly under strong interventions. A scaling-invariance stress test confirms that our method is robust to function-preserving reparameterizations that break variance-based selection.

All proofs are deferred to Appendix A.

2. Related Work

Causal abstraction. The theoretical foundations for relating causal models at different granularities were laid by Rubenstein et al. (2017), who formalize *exact transformations* between SEMs, and by Beckers and Halpern (2019), who develop a hierarchy of abstraction notions based on state maps τ and intervention maps ω . Beckers et al. (2020) extend this to *approximate* abstractions suitable for realistic systems with graded mismatches. More recently, Massidda et al. (2023) generalize the framework to soft interventions where mechanisms are replaced by functions rather than con-

stants, and Geiger et al. (2025) connect causal abstraction to the broader mechanistic interpretability program.

Interchange interventions for neural networks. Geiger et al. (2021) operationalize causal abstraction for neural networks via *interchange interventions*, which swap internal activations between inputs to test whether neural variables behave like high-level causal variables; they propose IIA as a graded faithfulness metric. Geiger et al. (2022) show that networks can be trained to realize a target causal structure, and that behavioral accuracy can mask mechanistic failures detectable only through IIA. Recent work addresses the *discovery* of alignments between high-level variables and distributed representations (Geiger et al., 2024), though scalable discovery for large pretrained networks remains open.

Structured pruning. Classical second-order methods like Optimal Brain Damage (LeCun et al., 1989) and Optimal Brain Surgeon (Hassibi and Stork, 1992) prune weights using curvature information. Structured approaches remove entire units based on activation statistics or redundancy (Sanh et al., 2020); variance-based pruning (VBP) is a recent instance that removes low-variance units with mean-shift compensation (Berisha et al., 2025). Neuron merging methods fold pruned units into retained ones (Kim et al., 2020). Our work differs in framing: we cast mechanism replacement as constructing an explicit causal abstraction and use interventional faithfulness—not just task accuracy—as the target.

3. Problem Setup: Constructive Abstraction Discovery via Mechanism Replacement

We formalize abstraction discovery as searching for a reduced SCM that approximately preserves the network’s behavior under a specified intervention family.

3.1. The network as a deterministic SCM

Let $f_\theta : \mathcal{X} \rightarrow \mathbb{R}^q$ be a trained feedforward network with parameters θ . Write $a^{(\ell)}(x) \in \mathbb{R}^{d_\ell}$ for the post-nonlinearity activations at layer ℓ and $\hat{y}(x) = f_\theta(x)$ for the output. We treat the network as a deterministic SCM $M_L = (\mathbf{U}, \mathbf{V}, \mathcal{F})$ with exogenous variable $X \in \mathbf{U}$ and endogenous variables $\mathbf{V} = \{a_j^{(\ell)}\}_{\ell,j} \cup \{\hat{Y}\}$. The structural equations are the forward computations:

$$z^{(\ell)} = W^{(\ell)} a^{(\ell-1)} + b^{(\ell)}, \quad a^{(\ell)} = \sigma^{(\ell)}(z^{(\ell)}), \quad \hat{Y} = f_\theta(X).$$

Labels Y are external to M_L and used only to evaluate task performance.

3.2. Constructive mechanism replacement

We build candidate high-level models by *mechanism replacement* on selected units, following the constructive abstraction framework of Beckers and Halpern (2019) and its soft-intervention extension (Massidda et al., 2023). For a unit $a_j^{(\ell)}$, we allow three operations: (i) **Keep**: preserve the original structural equation; (ii) **Hard replacement**: set $a_j^{(\ell)} := c$ for a constant c ; (iii) **Soft replacement**: set $a_j^{(\ell)} := \beta + \sum_{k \in P} w_k a_k^{(\ell)}$ for a small index set P of retained units. Applying replacements to a set S of units yields a modified SCM denoted $M_H(S, \eta)$, where η collects the replacement parameters.

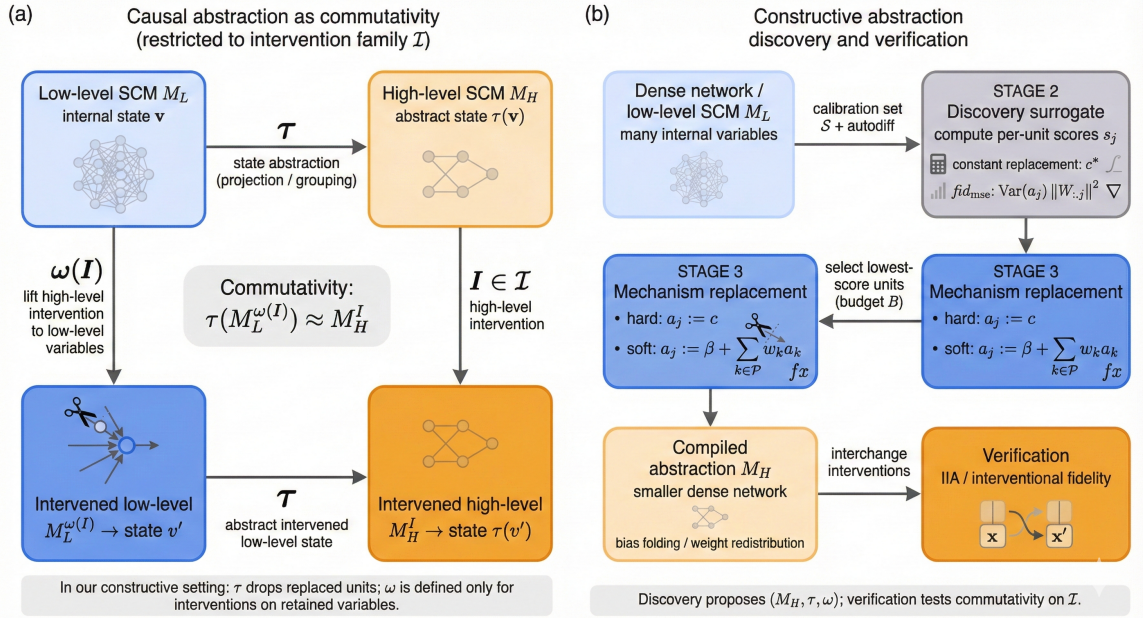


Figure 1: Overview. (a) Causal abstraction as commutativity: a high-level SCM M_H abstracts a low-level model M_L if intervening at the high level (via \mathcal{I}) and intervening at the low level (via $\omega(\mathcal{I})$) yield consistent results under the state map τ . (b) Our discovery and verification pipeline: given a dense network, we compute per-unit scores s_j via a second-order surrogate, select low-score units for mechanism replacement, compile the result into a smaller network M_H , and verify faithfulness via interchange interventions (IIA).

Terminological note: two senses of “intervention.” Throughout this paper, the word *intervention* appears in two distinct roles. *Mechanism-replacement interventions* (hard or soft) modify the structural equations of the network to produce a reduced model; these are the constructive operations used during **discovery** (Sections 4–6). *Interchange interventions* swap activations between inputs to test commutativity; these are the diagnostic operations used during **verification** (Section 7). Where ambiguity could arise, we use the qualified terms explicitly.

3.3. Abstraction maps and commutativity

A causal abstraction requires a state map τ and an intervention map ω (Beckers and Halpern, 2019). Intuitively, τ “forgets” the replaced variables, and ω ensures that when we intervene on a high-level variable, we intervene on the corresponding low-level unit in the same way. In our setting, τ projects onto retained variables (discarding replaced ones), and ω is defined for interventions targeting retained variables—mapping each high-level intervention to the corresponding low-level intervention on the same units.¹

For deterministic models, exact commutativity on an intervention family \mathcal{I} requires

$$\tau\left(M_L^{\omega(I)}(x)\right) = M_H^I(x) \quad \forall x \in \mathcal{X}, \forall I \in \mathcal{I}. \quad (1)$$

1. Interventions on replaced variables are not representable at the high level, consistent with constructive abstraction definitions (Beckers et al., 2020).

Since this rarely holds exactly, we work with approximate commutativity. Given a discrepancy $d(\cdot, \cdot)$ on outcomes, define the interventional risk

$$\mathcal{L}_{\mathcal{I}}(M_H; M_L) := \mathbb{E}_{x \sim \mathcal{D}} \mathbb{E}_{I \sim \mathcal{I}} \left[d\left(\tau(M_L^{\omega(I)}(x)), M_H^I(x)\right) \right]. \quad (2)$$

When d is the 0–1 mismatch indicator under interchange interventions, $1 - \mathcal{L}_{\mathcal{I}}$ recovers IIA (Geiger et al., 2021).

Abstraction class and intervention family. Throughout, we focus on *layerwise projection abstractions* induced by mechanism replacement at a fixed layer ℓ : we choose a retained index set $K \subseteq \{1, \dots, d_\ell\}$ and replace the remaining coordinates $S = K^c$ by either constants or functions of $a_K^{(\ell)}$ (Section 3.2). The state map τ is the projection onto retained variables (and the output), $\tau(a^{(\ell)}) := a_K^{(\ell)}$, and the intervention map ω acts as the identity on interventions targeting retained coordinates.

In experiments, the intervention family \mathcal{I} consists of *interchange interventions* on *retained* coordinates only: given two inputs (x, x') and a mask $m \in \{0, 1\}^{|K|}$, we intervene by setting

$$\tilde{a}_K^{(\ell)} = m \odot a_K^{(\ell)}(x') + (1 - m) \odot a_K^{(\ell)}(x),$$

and then continuing the forward computation. Interventions on replaced variables are intentionally excluded from \mathcal{I} (they are not representable at the high level), consistent with constructive abstraction definitions (Beckers et al., 2020).

3.4. Discovery objective

We seek a sparse high-level model faithful under \mathcal{I} :

$$\min_{S, \eta} \mathcal{L}_{\mathcal{I}}(M_H(S, \eta); M_L) \quad \text{s.t.} \quad |S| \geq d_\ell - K, \quad (3)$$

where K bounds the number of retained variables. Direct optimization via interchange interventions is expensive; we instead derive a second-order surrogate for the task-loss change induced by mechanism replacement (Section 5), yielding per-unit scores that efficiently identify candidate abstractions for subsequent IIA verification. Figure 1 summarizes the abstraction framework and our discovery pipeline.

Roadmap. Since directly optimizing the interventional risk (2) is combinatorially expensive, our approach proceeds in three stages: (1) a second-order Taylor surrogate approximates the task-loss change from each mechanism replacement, yielding closed-form scores in a single autodiff pass (Section 5); (2) low-score units are compiled out to form a candidate abstraction (Section 6); (3) the candidate is validated via interchange interventions using the gold-standard IIA criterion (Section 7). The surrogate is *not* an approximation to IIA itself but a cheap filter whose minima correlate with high IIA.

4. Compilation of Mechanism Replacements

The mechanism replacements introduced in Section 3 can be *compiled* into smaller dense networks without runtime masking. This makes the constructed abstraction operational and efficient.

Consider the downstream affine map $z^{(\ell+1)} = W^{(\ell+1)}a^{(\ell)} + b^{(\ell+1)}$.

Proposition 1 (Bias folding for constant replacement) *Under $\text{do}(a_j^{(\ell)} := c)$, let $W' := W_{:, \setminus j}^{(\ell+1)}$ and $b' := b^{(\ell+1)} + cW_{:, j}^{(\ell+1)}$. Then $W^{(\ell+1)}a^{(\ell)} + b^{(\ell+1)} \Big|_{a_j^{(\ell)}=c} = W'a_{\setminus j}^{(\ell)} + b'$.*

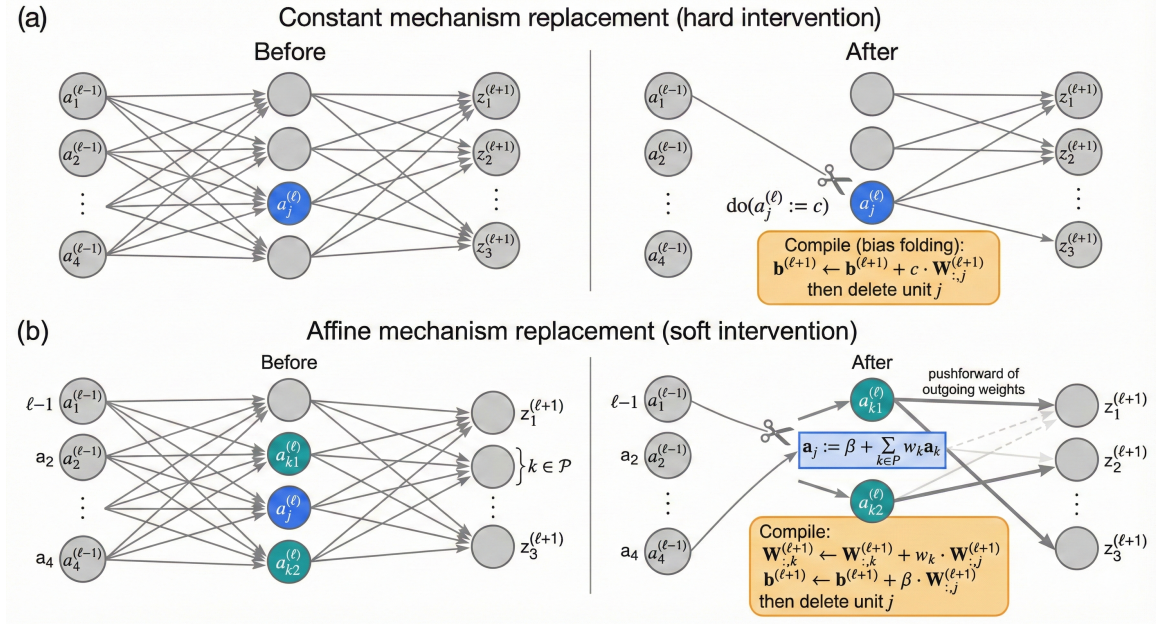


Figure 2: Compilation of mechanism replacements. (a) Constant replacement: setting $a_j^{(\ell)} := c$ severs incoming edges; the effect on downstream units is absorbed into the bias via $\mathbf{b}^{(\ell+1)} \leftarrow \mathbf{b}^{(\ell+1)} + c \cdot \mathbf{W}_{:,j}^{(\ell+1)}$, then column j is deleted. (b) Affine replacement: replacing a_j with a linear combination of retained units $\{a_k\}_{k \in P}$ redistributes outgoing weights to those units before deletion.

This is the mean-shift compensation used in structured pruning (Berisha et al., 2025). Figure 2(a) illustrates the operation.

Proposition 2 (Weight folding for affine replacement) Under $\text{do}(a_j^{(\ell)} := \beta + \sum_{k \in P} w_k a_k^{(\ell)})$, let $\mathbf{W}'_{:,k} := \mathbf{W}_{:,k}^{(\ell+1)} + w_k \mathbf{W}_{:,j}^{(\ell+1)}$ for $k \in P$, let $\mathbf{b}' := \mathbf{b}^{(\ell+1)} + \beta \mathbf{W}_{:,j}^{(\ell+1)}$, and remove column j . Then the downstream pre-activation is preserved exactly.

This generalizes neuron merging (Kim et al., 2020); see Figure 2(b).

Lemma 3 (Exact transformation) Let $M_H(S, \eta)$ be the compiled network after applying replacements to units S with parameters η . Then $f_{M_H(S, \eta)}(x) = f_{M_L^{\text{do}(S; \eta)}}(x)$ for all x —compilation is an exact transformation of the intervened SCM (Rubenstein et al., 2017).

The proof follows by composing the exact pre-activation identities from Propositions 1–2 (Appendix A.7).

5. A Tractable Surrogate for Constructive Abstraction Discovery

Directly optimizing the interventional objective (3) requires many explicit interventions and is expensive (Geiger et al., 2021). We derive a tractable surrogate by approximating the task-loss change induced by mechanism replacement.

5.1. Task-grounded risk and second-order proxy

Let $\mathcal{D}_{\text{cal}} = \{(x_s, y_s)\}_{s=1}^n$ be a calibration set with baseline risk $L(\theta) := \frac{1}{n} \sum_s \ell(f_\theta(x_s), y_s)$. For an intervention I , write $\Delta L^I := L^I(\theta) - L(\theta)$ for the induced risk change. Replacements with small ΔL^I preserve task behavior.

Fix a unit (ℓ, j) and consider hard replacement $\text{do}(a_j^{(\ell)} := c)$. Let $A_{s,j}$ denote the observed activation on sample s , and define $\delta_s(c) := c - A_{s,j}$. Let $g_s := \partial L_s / \partial A_{s,j}$ and $h_s := \partial^2 L_s / \partial A_{s,j}^2$ be the per-sample gradient and curvature.

Proposition 4 (Quadratic proxy) *A second-order expansion yields*

$$\Delta L^{\text{do}(a_j^{(\ell)} := c)} \approx \widehat{\Delta L}_j(c) := \frac{1}{n} \sum_s g_s \delta_s(c) + \frac{1}{2n} \sum_s h_s \delta_s(c)^2. \quad (4)$$

Proposition 5 (Optimal constant) *Assuming $\sum_s h_s > 0$, the minimizer of $\widehat{\Delta L}_j(c)$ is*

$$c_j^* = \underbrace{\frac{\sum_s h_s A_{s,j}}{\sum_s h_s}}_{\text{curvature-weighted mean}} - \underbrace{\frac{\sum_s g_s}{\sum_s h_s}}_{\text{gradient correction}}. \quad (5)$$

The unit score $s_j := \widehat{\Delta L}_j(c_j^*)$ quantifies the minimal proxy cost of replacing unit j .

The derivation (Appendix A, Section A.2) follows by setting $\frac{\partial}{\partial c} \widehat{\Delta L}_j(c) = 0$.

When does $\sum_s h_s > 0$ hold? The condition $\sum_s h_s > 0$ ensures the quadratic proxy is strictly convex in c so that a unique minimizer exists. In our main experimental setting—cross-entropy loss with a linear head at the penultimate layer—each per-sample curvature is $h_{s,j} = W_{:,j}^\top (\text{Diag}(p_s) - p_s p_s^\top) W_{:,j}$, which is nonnegative because $\text{Diag}(p_s) - p_s p_s^\top$ is the covariance of a categorical distribution and hence positive semidefinite. The sum $\sum_s h_s$ is strictly positive as long as $W_{:,j} \neq 0$ and the softmax outputs are non-degenerate on at least one calibration sample. This holds generically for trained networks with nonzero output weights.

In rare degenerate cases where the total curvature is very small (e.g., a near-dead unit with $W_{:,j} \approx 0$), the unit has negligible effect on the output regardless of its value, so any replacement constant suffices and the unit can be removed at near-zero cost. In practice, we add a small ridge $\epsilon = 10^{-8}$ to the denominator to ensure numerical stability.

5.2. Connection to variance-based pruning

Proposition 6 (Variance ranking as a special case) *Under (i) stationarity ($\sum_s g_s = 0$) and (ii) uniform curvature ($h_s = \alpha > 0$), the optimal constant is the mean \bar{A}_j and the score becomes $s_j = \frac{\alpha}{2} \text{Var}(A_{:,j})$.*

The proof is immediate by substituting the assumptions into (5) (Appendix A.8).

Thus VBP (Berisha et al., 2025) implicitly assumes uniform curvature, reducing interventional scoring to variance ranking.

5.3. Affine replacements

Affine replacements $a_j := \beta + \sum_{k \in P} w_k a_k$ generalize constant replacement by approximating a removed unit as a function of retained units. To apply Proposition 7 below, one must specify a *parent set* $P \subseteq K$ of retained units used in the affine surrogate.

Parent-set selection. In practice, we choose P as the top- r retained units ranked by absolute Pearson correlation with a_j on the calibration set \mathcal{D}_{cal} . That is, $P = \text{top-}r_{k \in K} |\widehat{\text{corr}}(A_{:,j}, A_{:,k})|$, where r is a small integer (e.g., $r \in \{2, 4, 8\}$). Correlation-based selection is fast (linear in $|K|$) and identifies the units most predictive of a_j . The affine fit then captures the linear component of a_j 's dependence on these parents; the residual becomes the replacement cost.

Weighted regression formulation. Let $\Phi \in \mathbb{R}^{n \times (|P|+1)}$ be the design matrix with columns $A_{:,k}$ for $k \in P$ and a column of ones (for the intercept β), let $\theta = (w_k)_{k \in P} \oplus \beta$ collect the affine parameters, and let $D = \text{Diag}(\mathbf{h})$ where $\mathbf{h} = (h_1, \dots, h_n)^\top$ are the per-sample curvatures.

Proposition 7 (Affine fit) *The optimal affine parameters minimizing the quadratic proxy (4) solve the weighted normal equations*

$$(\Phi^\top D \Phi) \theta^* = \Phi^\top (D \mathbf{a} - \mathbf{g}), \quad (6)$$

where $\mathbf{a} = A_{:,j}$ and $\mathbf{g} = (g_1, \dots, g_n)^\top$. When the model is near a stationary point ($\mathbf{g} \approx 0$), this reduces to curvature-weighted least squares: $\theta^* \approx (\Phi^\top D \Phi)^{-1} \Phi^\top D \mathbf{a}$.

The proof follows by differentiating the quadratic proxy with respect to θ (see Appendix A, Section A.3). When $P = \emptyset$, the normal equations recover Proposition 5: constant replacement is the $|P| = 0$ special case. Affine replacements are compiled via weight folding (Proposition 2); in experiments, we use bias folding by default and activate weight folding only when the affine score is strictly lower.

5.4. Multi-unit selection

Joint selection of multiple units couples through cross-unit interaction terms. The exact joint proxy for replacing a set S simultaneously involves the full $|S| \times |S|$ cross-Hessian $H_{jk} = \frac{1}{n} \sum_s \frac{\partial^2 L_s}{\partial A_{s,j} \partial A_{s,k}}$. We adopt a standard diagonal approximation:

Assumption 8 (Diagonal interactions) *The cross-Hessian of calibration risk with respect to activation perturbations at different units is approximately zero: $H_{jk} \approx 0$ for $j \neq k$. Concretely, this means that the task-loss curvature induced by perturbing unit j does not depend strongly on simultaneous perturbations of unit k , so the joint cost of replacing a set S approximately decomposes into a sum of single-unit costs.*

This is the activation-space analogue of the diagonal Hessian assumption used in OBD (LeCun et al., 1989). It holds exactly when the loss landscape has axis-aligned curvature in the activation basis, and approximately when cross-unit interactions are weak relative to self-interactions. In our setting (penultimate layer before a linear classifier with cross-entropy loss), the curvature factorizes through the output weight matrix: $H_{jk} = \frac{1}{n} \sum_s W_{:,j}^\top (\text{Diag}(p_s) - p_s p_s^\top) W_{:,k}$, which is small when the output weight columns $W_{:,j}$ and $W_{:,k}$ are approximately orthogonal. Systematically validating additivity beyond this analytic motivation is an interesting direction for future work.

Proposition 9 (Additive scores) *Under Assumption 8, $\widehat{\Delta L}(S) \approx \sum_{j \in S} s_j$, so selecting units with the m smallest scores is proxy-optimal for the joint replacement problem.*

The proof (Appendix A.4) shows that cross terms vanish under Assumption 8, leaving independently minimizable single-unit costs.

This yields a scalable procedure: compute per-unit scores via autodiff on the calibration set \mathcal{D}_{cal} , select low-score units, and compile them out (Section 4).

6. Abstraction Discovery as Score-Based Search over Constructive Operators

The surrogate scores from Section 5 reduce abstraction discovery to a simple selection problem. Under the diagonal approximation (Assumption 8), scores are additive, so selecting units with the m smallest scores is proxy-optimal for removing m units. Algorithm 1 summarizes the procedure.

The algorithm is a *discovery* procedure that proposes candidate abstractions; verification of faithfulness under interchange interventions is handled separately (Section 7).

7. Interventional Verification of the Discovered Abstraction

Discovery proposes a candidate abstraction (M_H, τ, ω) ; verification tests whether commutativity holds on an intervention family \mathcal{I} . Following Geiger et al. (2021), we use interchange interventions.

Interchange interventions. Given retained coordinates K at layer ℓ , an interchange intervention takes two inputs (x, x') and a mask $m \in \{0, 1\}^{|K|}$, forming a hybrid activation $\tilde{a}_K = m \odot a_K(x') + (1 - m) \odot a_K(x)$ that replaces $a_K(x)$ before running the forward pass. We measure agreement between the low-level and high-level models under the same intervention.

Interventional fidelity. Let $d(\cdot, \cdot) \in [0, 1]$ be a discrepancy (e.g., 0–1 mismatch for predicted class). Define

$$\text{IF}(M_H; M_L, \mathcal{I}) := \mathbb{E}_{I \sim \mathcal{I}} [d(M_H^I, \tau(M_L^{\omega(I)}))]. \quad (7)$$

When d is the 0–1 indicator, $1 - \text{IF}$ is the interchange intervention accuracy (IIA) of Geiger et al. (2021). In practice, we estimate IF from R sampled interventions; by Hoeffding’s inequality, the empirical estimate concentrates within $O(1/\sqrt{R})$ of the true value, justifying confidence intervals.

Two-stage approach. Our task-grounded surrogate (Section 5) does not directly optimize IF, but serves as a cheap filter: it proposes candidates that are then validated via IIA on \mathcal{I} . This separation keeps discovery tractable while ensuring verification uses the gold-standard interventional criterion.

8. Experiments

Our experiments assess whether abstractions discovered by the constructive mechanism-replacement operators (Sections 4–6) are *faithful under interventions*. Faithfulness is evaluated using interchange-style commutativity tests commonly used in causal abstraction for neural networks (Geiger et al., 2021, 2025). We focus on settings where both discovery and verification are computationally light, allowing experiments to run under tight time constraints.

8.1. Setup

Datasets. We use MNIST handwritten digits (Lecun et al., 1998) with the standard train/test split (60k/10k). Inputs are normalized using standard MNIST statistics, following common torchvision baselines. As a controlled sanity check, we also include a small synthetic Boolean circuit task, described below.

Models. For MNIST, we train a three-layer MLP with ReLU activations: $784 \rightarrow 512 \rightarrow 512 \rightarrow 10$. Abstractions are constructed at the *penultimate* activation vector $a \in \mathbb{R}^{512}$, immediately before the final linear classifier. This choice makes compilation exact and evaluation fast (Proposition 1).

Algorithm 1: Constructive abstraction discovery

Input : Network f_θ ; calibration \mathcal{D}_{cal} ; budget B
Output: Compiled reduced model M_H ; projection τ
 Compute per-unit $g_{s,j}, h_{s,j}$ on \mathcal{D}_{cal} via autodiff
foreach unit j **do**
 Compute c_j^* via (5) and score s_j
 if affine enabled **then**
 Solve (6) for each parent set P
 If affine score $< s_j$: use affine
 end
end
 $S \leftarrow B$ smallest-score indices
 Compile M_H via bias/weight folding
return M_H, τ

Calibration and budgets. Discovery uses a calibration set of $n_{\text{cal}} = 2000$ training examples, fixed per seed. For the main MNIST fidelity results, we report two representative keep budgets $\{384, 256\}$ at the penultimate layer (Section 8.2). For the invariance stress test, we report keep $\in \{384, 256\}$ under exact scaling reparameterizations (Section 8.3). For affine replacements, we focus on aggressive keep budgets $\{128, 64\}$ where soft mechanism replacement is most likely to matter (Section 8.5). Unless otherwise noted, MNIST results are averaged over 10 random seeds $\{0, \dots, 9\}$ and reported as mean \pm standard deviation.

Efficient computation. At the penultimate layer before a linear classifier with cross-entropy loss, per-sample gradients $g_{s,j}$ and curvatures $h_{s,j}$ admit closed forms involving only the softmax outputs and the output weight column $W_{:,j}$ (see Appendix A.6), so no second-order autodiff is required.

Baselines and methods. We compare the following approaches:

- **VBP:** variance-based structured pruning with mean replacement, which removes low-variance units (Berisha et al., 2025).
- **Random:** random unit removal with mean replacement, serving as a lower bound.
- **cwvar:** curvature-weighted variance (Section 5.2), using a curvature-weighted mean constant and a curvature-weighted variance score.
- **Logit-MSE (ours):** a label-free fidelity objective measuring the expected squared logit distortion induced by mechanism replacement at the penultimate layer. Let logits be $z = Wa + b$. Under constant replacement of unit j by its mean, the expected squared logit error contributed by unit j is proportional to

$$s_j^{\text{lm}} \propto \text{Var}(a_j) \|W_{:,j}\|_2^2. \quad (8)$$

The Logit-MSE method prunes units with the smallest score (8) and compiles replacements via bias folding (Proposition 1).

The score (8) measures the expected squared logit distortion from mean replacement (derivation in Appendix A.5). It is invariant to the ReLU scaling symmetry $a_j \mapsto sa_j$, $W_{:,j} \mapsto W_{:,j}/s$, which preserves $\text{Var}(a_j) \|W_{:,j}\|_2^2$.

Verification metrics (interventional fidelity). We report three metrics: (1) **Task accuracy** (test accuracy on MNIST); (2) **IIA-like fidelity**, comparing the predicted class of the dense model and compiled abstraction under interchange interventions on retained penultimate coordinates, averaged over $R = 2000$ random instances (Geiger et al., 2021); and (3) **KL fidelity**, $\text{KL}(p_{\text{dense}} \| p_{\text{abs}})$ between predictive distributions under the same interventions (lower is better). We focus on Bernoulli masks with swap probability $p = 0.5$ as a strong-intervention stress test; weaker swaps behave similarly but are less diagnostic.

8.2. MNIST: fidelity-complexity tradeoffs

Figure 3 and Table 1 report accuracy and interventional fidelity for two representative keep budgets. At keep = 384 and strong swaps ($p = 0.5$), Logit-MSE achieves slightly higher fidelity than VBP with comparable KL and identical accuracy (≈ 0.98). At keep = 256, IIA differences between Logit-MSE and VBP remain small, but Logit-MSE improves KL fidelity. Paired bootstrap tests confirm that the IIA deltas at keep $\in \{384, 256\}$ are not statistically significant (95% CIs cross 0), while the KL improvement at keep = 256 is significant (95% CI for $\Delta\text{KL} [-0.0420, -0.0187]$).

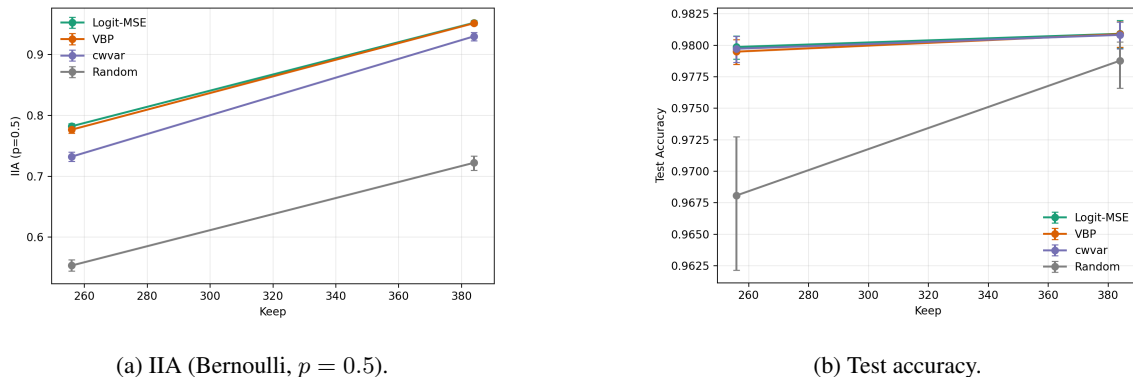


Figure 3: MNIST fidelity and accuracy vs. keep size. Fidelity is measured via interchange interventions on retained penultimate coordinates.

Keep	Method	Test Acc.	IIA ($p=0.5$)	KL ($p=0.5$)
384	Logit-MSE	0.981 ± 0.002	0.952 ± 0.006	0.035 ± 0.007
	VBP	0.981 ± 0.002	0.951 ± 0.004	0.038 ± 0.007
	cwvar	0.981 ± 0.002	0.930 ± 0.011	0.084 ± 0.023
256	Logit-MSE	0.980 ± 0.001	0.782 ± 0.006	0.578 ± 0.020
	VBP	0.979 ± 0.002	0.776 ± 0.010	0.609 ± 0.026
	cwvar	0.980 ± 0.002	0.732 ± 0.012	0.861 ± 0.087

Table 1: MNIST baseline summary (mean \pm std over seeds 0–9).

8.3. Exact reparameterization stress test: scaling invariance

A discovery criterion should depend on a model’s *causal behavior*—not on the coordinate system of its activations. Function-preserving reparameterizations (e.g., rescaling a hidden unit and inversely rescaling its outgoing weights) change activation magnitudes and variances without altering any input-output or interventional behavior; a criterion that selects different units afterward is confounding coordinate conventions with causal structure. This matters because different training runs and optimizers can produce networks related by such symmetries (Geiger et al., 2024).

To test this, we apply an exact function-preserving reparameterization of the trained MNIST MLP. Each penultimate unit is rescaled by a positive factor $s_j > 0$, with the inverse scaling applied to the corresponding output weights. Because ReLU is positively homogeneous, this transformation preserves the computed function exactly for all inputs. We sample s_j independently from a log-uniform distribution over the ranges $[0.1, 10]$ and $[0.01, 100]$, and rerun abstraction discovery and interchange verification on the reparameterized network.

Selection stability. We quantify stability using the Jaccard similarity between the sets of *kept* units in the original and reparameterized networks: $\text{Jaccard}(K, K') = \frac{|K \cap K'|}{|K \cup K'|}$.

Findings. Figure 4 and Table 2 show a clear separation. Logit-MSE is exactly invariant in this setting: the kept set is unchanged (Jaccard = 1.0), and strong-swap fidelity remains high under both scale ranges. In contrast, VBP is not invariant: at keep = 256 its kept-set Jaccard drops to 0.401 under $[0.01, 100]$ scaling and 0.451 under $[0.1, 10]$ scaling, and its interchange fidelity degrades substantially (e.g., IIA 0.592 and KL 1.647 under $[0.01, 100]$ scaling). This converts the invariance theorem into a concrete practical failure mode: a variance-only discovery criterion can produce

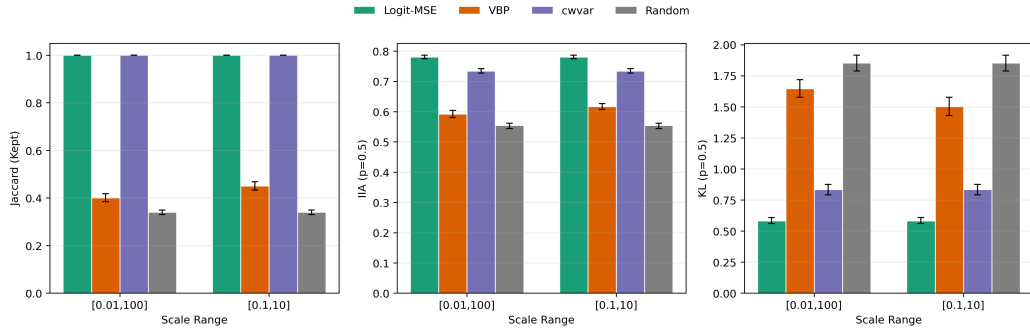


Figure 4: Scaling invariance stress test (keep = 256). Absolute metrics under exact function-preserving scaling reparameterizations (mean with 95% CI over 10 seeds). Logit-MSE (and cwvar) are stable (Jaccard = 1) and maintain strong-swap fidelity, while VBP is unstable and substantially less faithful under interventions.

Scale range	Method	Jaccard (kept)	IIA ($p=0.5$)	KL ($p=0.5$)
[0.01, 100]	Logit-MSE	1.000 [1.000, 1.000]	0.781 [0.775, 0.787]	0.582 [0.560, 0.608]
	VBP	0.401 [0.384, 0.418]	0.592 [0.580, 0.604]	1.647 [1.576, 1.719]
	cwvar	1.000 [1.000, 1.000]	0.735 [0.727, 0.742]	0.833 [0.791, 0.875]
	Random	0.340 [0.331, 0.349]	0.554 [0.544, 0.562]	1.852 [1.788, 1.916]
[0.1, 10]	Logit-MSE	1.000 [1.000, 1.000]	0.781 [0.775, 0.787]	0.582 [0.560, 0.608]
	VBP	0.451 [0.433, 0.468]	0.617 [0.607, 0.626]	1.502 [1.430, 1.577]
	cwvar	1.000 [1.000, 1.000]	0.735 [0.727, 0.742]	0.833 [0.791, 0.875]
	Random	0.340 [0.331, 0.349]	0.554 [0.544, 0.562]	1.852 [1.788, 1.916]

Table 2: Reparameterization invariance at keep = 256 (mean [95% CI] over 10 seeds; values rounded to 3 decimals).

different abstractions for functionally identical networks, and those abstractions are less faithful under interventions.

8.4. Boolean circuit sanity check

We also evaluate a synthetic Boolean task with inputs $x \in \{0, 1\}^8$ and a compositional label $y = \text{XOR}(\text{AND}(x_1, x_2), \text{OR}(x_3, x_4))$. The dataset contains 4096 examples with an 80/20 train-test split. We train a small ReLU MLP $8 \rightarrow 64 \rightarrow 64 \rightarrow 2$ and apply the same abstraction pipeline at the penultimate layer. This task serves as a controlled check that discovery, compilation, and interchange evaluation behave as expected in a setting with an explicit compositional mechanism.

Quantitative results. Across 6 seeds (0–5) with $R = 2000$ interventions per seed, Logit-MSE performs competitively under interchange verification. For example: (i) at keep = 32, Logit-MSE achieves $\text{IIA} = 0.9268 \pm 0.0196$ and $\text{KL} = 0.1724 \pm 0.0916$, versus VBP 0.9229 ± 0.0249 and 0.2344 ± 0.1488 ; (ii) at keep = 16, Logit-MSE attains higher accuracy (0.9872 ± 0.0286) than VBP (0.9510 ± 0.0501), with similar IIA/KL in this regime.

8.5. Affine mechanism replacement improves fidelity at fixed keep size

Constant replacement is the simplest constructive operator, but Section 5.3 predicts that *soft* (affine) replacements can reduce proxy risk by approximating removed variables as functions of retained ones. To test this, we fix a keep size $|K|$ and compare two compiled abstractions: (i) constant replacement for all removed units $S = K^c$, and (ii) affine replacement where each removed unit a_j is approximated by an affine function of a small parent set $a_j \approx \beta_j + \sum_{k \in P_j} w_{j,k} a_k$ with $P_j \subseteq K$.

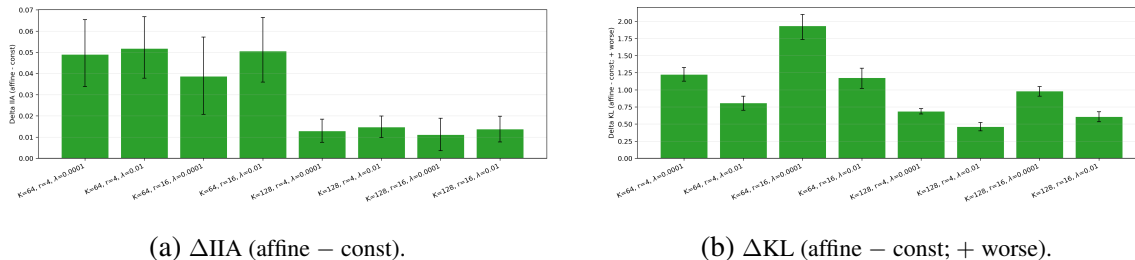
(a) ΔIIA (affine - const).(b) ΔKL (affine - const; + worse).

Figure 5: Affine vs. constant replacement (MNIST, $p = 0.5$ swaps). Affine replacement improves IIA at aggressive keep budgets, while increasing KL in these configurations.

Parent sets P_j are chosen as the top- r retained units by absolute correlation with a_j on the calibration set, and affine parameters are fit by minimizing the quadratic proxy (Proposition 7). We then compile the resulting abstraction via weight folding (Proposition 2) and evaluate fidelity under the same interchange interventions. We expect affine replacement to yield the largest gains under strong interventions (larger p) and more aggressive pruning (smaller $|K|$).

Results and tradeoff. Figure 5 shows that affine replacement can improve IIA under aggressive budgets. At $\text{keep} = 64$, using $r = 16$ correlated parents with ridge 10^{-2} yields $\Delta IIA = +0.0506$ with 95% CI $[0.0359, 0.0664]$ (affine minus constant) over 10 seeds. However, affine replacement increases KL in these configurations ($\Delta KL = +1.1775$ with 95% CI $[1.0215, 1.3148]$ at the same setting), so it should be viewed as a controllable fidelity tradeoff rather than a uniformly dominant replacement.

Computational cost. Appendix C reports wall-clock timings for scoring, compilation, and verification. The key takeaway is that scoring is a single forward-pass computation, while verification under interchange interventions dominates runtime at $R = 2000$.

9. Conclusion

We have shown that structured pruning can be understood as constructing a causal abstraction, with mechanism replacement providing the formal link between removing neural network units and producing a reduced SCM. The second-order surrogate makes discovery tractable, and the connection to variance-based pruning clarifies both the success of that heuristic (when curvature is uniform) and its failure modes (under reparameterization). Our experiments confirm that targeting interventional fidelity rather than activation statistics alone yields more robust abstractions. Looking ahead, extending this framework to attention mechanisms, multi-layer abstractions, and soft interventions beyond affine surrogates would broaden its applicability to modern architectures.

References

- Sander Beckers and Joseph Y. Halpern. Abstracting causal models. In *Proceedings of the AAAI Conference on Artificial Intelligence*, volume 33, pages 2678–2685, 2019. doi: 10.1609/aaai.v33i01.33012678.
- Sander Beckers, Frederick Eberhardt, and Joseph Y. Halpern. Approximate causal abstractions. In *Proceedings of the Thirty-Fifth Conference on Uncertainty in Artificial Intelligence (UAI 2019)*, volume 115 of *Proceedings of Machine Learning Research*, pages 606–615. AUAI Press, 2020.

- Uranik Berisha, Jens Mehnert, and Alexandru Paul Condurache. Variance-based pruning for accelerating and compressing trained networks. In *Proceedings of the IEEE/CVF International Conference on Computer Vision (ICCV)*, pages 4973–4982, 2025.
- Atticus Geiger, Hanson Lu, Thomas Icard, and Christopher Potts. Causal abstractions of neural networks. In *Advances in Neural Information Processing Systems*, 2021.
- Atticus Geiger, Zhengxuan Wu, Hanson Lu, Josh Rozner, Elisa Kreiss, Thomas Icard, Noah D. Goodman, and Christopher Potts. Inducing causal structure for interpretable neural networks. In *Proceedings of the 39th International Conference on Machine Learning*, volume 162 of *Proceedings of Machine Learning Research*, pages 7324–7338. PMLR, 2022.
- Atticus Geiger, Zhengxuan Wu, Christopher Potts, Thomas Icard, and Noah D. Goodman. Finding alignments between interpretable causal variables and distributed neural representations. In *Proceedings of the Third Conference on Causal Learning and Reasoning*, volume 236 of *Proceedings of Machine Learning Research*, pages 160–187. PMLR, 2024.
- Atticus Geiger, Duligur Ibeling, Amir Zur, Maheep Chaudhary, Sonakshi Chauhan, Jing Huang, Aryaman Arora, Zhengxuan Wu, Noah D. Goodman, Christopher Potts, and Thomas Icard. Causal abstraction: A theoretical foundation for mechanistic interpretability. *Journal of Machine Learning Research*, 26(83):1–64, 2025.
- Babak Hassibi and David G. Stork. Second order derivatives for network pruning: Optimal brain surgeon. In *Advances in Neural Information Processing Systems*, volume 5, pages 164–171. Morgan Kaufmann, 1992.
- Woojeong Kim, Suhyun Kim, Mincheol Park, and Geunseok Jeon. Neuron merging: Compensating for pruned neurons. In *Advances in Neural Information Processing Systems*, 2020.
- Y. Lecun, Léon Bottou, Yoshua Bengio, and Patrick Haffner. Gradient-based learning applied to document recognition. *Proceedings of the IEEE*, 86(11):2278–2324, 1998. doi: 10.1109/5.726791.
- Yann LeCun, John S. Denker, and Sara A. Solla. Optimal brain damage. In *Advances in Neural Information Processing Systems*, volume 2, pages 598–605. Morgan Kaufmann, 1989.
- Riccardo Massidda, Atticus Geiger, Thomas Icard, and Davide Bacciu. Causal abstraction with soft interventions. In *Proceedings of the Second Conference on Causal Learning and Reasoning*, volume 213 of *Proceedings of Machine Learning Research*, pages 68–87. PMLR, 2023.
- Chris Olah, Nick Cammarata, Ludwig Schubert, Gabriel Goh, Michael Petrov, and Shan Carter. Zoom in: An introduction to circuits. *Distill*, 5(3), 2020. doi: 10.23915/distill.00024.001.
- Judea Pearl. *Causality*. Cambridge University Press, 2 edition, 2009. doi: 10.1017/CBO9780511803161.
- Paul K. Rubenstein, Sebastian Weichwald, Stephan Bongers, Joris M. Mooij, Dominik Janzing, Moritz Grosse-Wentrup, and Bernhard Schölkopf. Causal consistency of structural equation models. In *Proceedings of the Thirty-Third Conference on Uncertainty in Artificial Intelligence (UAI 2017)*. AUAI Press, 2017.

Victor Sanh, Thomas Wolf, and Alexander M. Rush. Movement pruning: Adaptive sparsity by fine-tuning. In *Advances in Neural Information Processing Systems*, 2020.

Appendix A. Detailed Derivations

A.1. Derivation of the Quadratic Proxy (Proposition 4)

Consider replacing unit (ℓ, j) with a constant c via $\text{do}(a_j^{(\ell)} := c)$. On calibration sample s , the activation changes from $A_{s,j}$ to c , inducing a perturbation $\delta_s(c) = c - A_{s,j}$. The loss change on sample s is

$$\Delta L_s(c) = L_s|_{a_j=c} - L_s|_{a_j=A_{s,j}}.$$

A second-order Taylor expansion around the observed activation gives

$$\Delta L_s(c) \approx g_s \cdot \delta_s(c) + \frac{1}{2} h_s \cdot \delta_s(c)^2,$$

where $g_s = \frac{\partial L_s}{\partial a_j} |_{a_j=A_{s,j}}$ and $h_s = \frac{\partial^2 L_s}{\partial a_j^2} |_{a_j=A_{s,j}}$. Averaging over the calibration set:

$$\widehat{\Delta L}_j(c) = \frac{1}{n} \sum_{s=1}^n \left[g_s \delta_s(c) + \frac{1}{2} h_s \delta_s(c)^2 \right].$$

A.2. Full Derivation: Optimal Constant and Score (Proposition 5)

Setting $\frac{\partial}{\partial c} \widehat{\Delta L}_j(c) = 0$:

$$\frac{1}{n} \sum_s g_s + \frac{1}{n} \sum_s h_s (c - A_{s,j}) = 0 \quad \Rightarrow \quad c \sum_s h_s = \sum_s h_s A_{s,j} - \sum_s g_s.$$

Dividing by $\sum_s h_s > 0$:

$$c_j^* = \frac{\sum_s h_s A_{s,j}}{\sum_s h_s} - \frac{\sum_s g_s}{\sum_s h_s}.$$

The first term is a curvature-weighted mean of the observed activations. The second term is a gradient correction that vanishes at stationarity ($\sum_s g_s = 0$).

The score $s_j = \widehat{\Delta L}_j(c_j^*)$ is the residual proxy cost after optimizing c . Substituting c_j^* back:

$$s_j = \frac{1}{2n} \sum_s h_s (c_j^* - A_{s,j})^2 + \frac{1}{n} \sum_s g_s (c_j^* - A_{s,j}).$$

Under stationarity, this simplifies to $s_j = \frac{1}{2n} \sum_s h_s (c_j^* - A_{s,j})^2$, a curvature-weighted variance.

A.3. Affine Normal Equations (Proposition 7)

Let $\hat{a}_j = \Phi \theta$ where $\Phi \in \mathbb{R}^{n \times (|P|+1)}$ has columns $A_{:,k}$ for $k \in P$ and a ones column, and $\theta = (w_P, \beta)$. The perturbation is $\delta = \Phi \theta - \mathbf{a}$ where $\mathbf{a} = A_{:,j}$. The quadratic proxy is:

$$\begin{aligned} \widehat{\Delta L}_j(\theta) &= \frac{1}{n} [\mathbf{g}^\top \delta + \frac{1}{2} \delta^\top D \delta] \\ &= \frac{1}{n} [\mathbf{g}^\top (\Phi \theta - \mathbf{a}) + \frac{1}{2} (\Phi \theta - \mathbf{a})^\top D (\Phi \theta - \mathbf{a})]. \end{aligned}$$

Taking the gradient with respect to θ :

$$\begin{aligned}\nabla_{\theta} \widehat{\Delta L}_j &= \frac{1}{n} \Phi^{\top} [\mathbf{g} + D(\Phi\theta - \mathbf{a})] = 0 \\ \Rightarrow \Phi^{\top} D \Phi \theta^* &= \Phi^{\top} (D \mathbf{a} - \mathbf{g}).\end{aligned}$$

The matrix $\Phi^{\top} D \Phi$ is symmetric positive definite when $D \succ 0$ and Φ has full column rank, ensuring a unique solution.

When $\mathbf{g} \approx 0$ (near stationarity), the solution reduces to $\theta^* = (\Phi^{\top} D \Phi)^{-1} \Phi^{\top} D \mathbf{a}$, which is curvature-weighted least-squares regression of a_j on the parent activations.

A.4. Additive Scores (Proposition 9)

The joint quadratic proxy for replacing set S with optimal constants is $\widehat{\Delta L}(S) = \frac{1}{n} \sum_s \sum_{j \in S} [g_{s,j} \delta_{s,j} + \frac{1}{2} h_{s,j} \delta_{s,j}^2] + \frac{1}{n} \sum_s \sum_{j \neq k \in S} H_{s,jk} \delta_{s,j} \delta_{s,k}$. Under Assumption 8, the cross terms vanish, giving $\widehat{\Delta L}(S) \approx \sum_{j \in S} s_j$. Since each s_j is independently minimized, the joint optimum is achieved by selecting the m smallest.

A.5. Derivation of the Logit-MSE Score

Because our abstractions are constructed at the penultimate layer $a \in \mathbb{R}^d$ immediately before the final linear map $z = Wa + b$, the effect of replacing a single coordinate a_j by a constant c on the logits is $z' - z = W_{:,j} (c - a_j)$. If we measure fidelity by squared logit error $d(z, z') = \|z - z'\|_2^2$ and choose $c = \mathbb{E}[a_j]$, then

$$\mathbb{E}[\|z' - z\|_2^2] = \mathbb{E}[(a_j - \mathbb{E}[a_j])^2] \|W_{:,j}\|_2^2 = \text{Var}(a_j) \|W_{:,j}\|_2^2,$$

which yields the score in Eq. (8) up to a constant factor.

A.6. Efficient Computation at the Penultimate Layer

At the penultimate layer a immediately before the final linear classifier $z = Wa + b$ with cross-entropy loss $\ell(z, y)$, the per-sample gradient with respect to activation coordinate a_j is

$$g_{s,j} = \frac{\partial \ell(z_s, y_s)}{\partial a_{s,j}} = W_{:,j}^{\top} (p_s - e_{y_s}),$$

where $p_s = \text{softmax}(z_s)$ and e_{y_s} is the one-hot vector for label y_s . The curvature term is

$$h_{s,j} = \frac{\partial^2 \ell(z_s, y_s)}{\partial a_{s,j}^2} = W_{:,j}^{\top} (\text{Diag}(p_s) - p_s p_s^{\top}) W_{:,j},$$

which is nonnegative because $\text{Diag}(p_s) - p_s p_s^{\top} \succeq 0$.

A.7. Exact Transformation (Lemma 3)

Each compilation step preserves downstream pre-activations exactly (Propositions 1–2). Composing over S yields functional equivalence: $f_{M_H(S,\eta)}(x) = f_{M_L^{\text{do}(S:=\eta)}}(x)$ for all x .

A.8. Variance Ranking as a Special Case (Proposition 6)

Under stationarity, $\sum_s g_s = 0$, so the gradient correction in (5) vanishes and $c_j^* = \bar{A}_j$. Under uniform curvature $h_s = \alpha > 0$:

$$s_j = \frac{1}{n} \sum_s \frac{\alpha}{2} (A_{s,j} - \bar{A}_j)^2 = \frac{\alpha}{2} \text{Var}(A_{:,j}).$$

Since α is constant across units, the ranking by s_j is identical to the ranking by $\text{Var}(A_{:,j})$.

Appendix B. Affine Replacement: Full Results

keep	r	ridge	metric	Δ (95% CI)	seeds	p
64	4	10^{-4}	IIA ($p=0.5$)	0.0490 [0.0338, 0.0653]	10	0.000
64	4	10^{-4}	KL ($p=0.5$)	1.2275 [1.1261, 1.3275]	10	0.000
64	4	10^{-4}	acc	0.0564 [0.0315, 0.0855]	10	0.004
64	4	10^{-2}	IIA ($p=0.5$)	0.0519 [0.0378, 0.0668]	10	0.000
64	4	10^{-2}	KL ($p=0.5$)	0.8086 [0.7022, 0.9076]	10	0.000
64	4	10^{-2}	acc	0.0564 [0.0320, 0.0847]	10	0.003
64	16	10^{-4}	IIA ($p=0.5$)	0.0387 [0.0207, 0.0571]	10	0.004
64	16	10^{-4}	KL ($p=0.5$)	1.9373 [1.7361, 2.1020]	10	0.000
64	16	10^{-4}	acc	0.0588 [0.0334, 0.0895]	10	0.004
64	16	10^{-2}	IIA ($p=0.5$)	0.0506 [0.0359, 0.0664]	10	0.000
64	16	10^{-2}	KL ($p=0.5$)	1.1775 [1.0215, 1.3148]	10	0.000
64	16	10^{-2}	acc	0.0588 [0.0334, 0.0893]	10	0.004
128	4	10^{-4}	IIA ($p=0.5$)	0.0130 [0.0075, 0.0184]	10	0.002
128	4	10^{-4}	KL ($p=0.5$)	0.6867 [0.6483, 0.7243]	10	0.000
128	4	10^{-4}	acc	0.0048 [0.0022, 0.0076]	10	0.008
128	4	10^{-2}	IIA ($p=0.5$)	0.0148 [0.0098, 0.0199]	10	0.000
128	4	10^{-2}	KL ($p=0.5$)	0.4629 [0.4019, 0.5224]	10	0.000
128	4	10^{-2}	acc	0.0051 [0.0025, 0.0079]	10	0.007
128	16	10^{-4}	IIA ($p=0.5$)	0.0112 [0.0036, 0.0189]	10	0.025
128	16	10^{-4}	KL ($p=0.5$)	0.9836 [0.9079, 1.0482]	10	0.000
128	16	10^{-4}	acc	0.0052 [0.0025, 0.0081]	10	0.008
128	16	10^{-2}	IIA ($p=0.5$)	0.0138 [0.0076, 0.0199]	10	0.002
128	16	10^{-2}	KL ($p=0.5$)	0.6082 [0.5335, 0.6795]	10	0.000
128	16	10^{-2}	acc	0.0054 [0.0027, 0.0082]	10	0.005

Appendix C. Timing Details

We report wall-clock timings for scoring, compilation, and verification. The verification step uses $R = 2000$ interventions, so it dominates runtime.

Environment note. Timings were collected in this run on CPU only; absolute values on a GPU machine may differ. *Interpretation.* Scoring is a single forward pass, verification dominates runtime ($R = 2000$ interventions), and affine compilation adds measurable overhead versus const.

keep	step	variant	mean \pm std	95% CI
128	compile	affine	0.3151 \pm 0.0280 s	[0.2990, 0.3336] s
256	compile	affine	0.2007 \pm 0.0164 s	[0.1915, 0.2120] s
128	compile	const	0.0000841 \pm 0.0000055 s	[0.0000807, 0.0000875] s
256	compile	const	0.0000751 \pm 0.0000079 s	[0.0000703, 0.0000800] s
all	score	logit_mse	0.1844 \pm 0.0455 s	[0.1645, 0.2163] s
128	verify	affine	0.004165 \pm 0.000368 s	[0.003944, 0.004399] s
256	verify	affine	0.005842 \pm 0.001113 s	[0.005237, 0.006600] s
128	verify	const	0.006269 \pm 0.001389 s	[0.005558, 0.007218] s
256	verify	const	0.007750 \pm 0.000831 s	[0.007222, 0.008256] s

Table 3: Wall-clock timing (seconds).